AERODYNAMIC COUPLING EFFECTS ON FLUTTER AND BUFFETING OF BRIDGES

By Xinzhong Chen,[1] Masaru Matsumoto,[2] and Ahsan Kareem,[3] Member, ASCE

ABSTRACT: The effects of aerodynamic coupling among modes of vibration on the flutter and buffeting response of long-span bridges are investigated. By introducing the unsteady, self-excited aerodynamic forces in terms of rational function approximations, the equations of motion in generalized modal coordinates are transformed into a frequency-independent state-space format. The frequencies, damping ratios, and complex mode shapes at a prescribed wind velocity, and the critical flutter conditions, are identified by solving a complex eigenvalue problem. A significant feature of this approach is that an iterative solution for determining the flutter conditions is not necessary, because the equations of motion are independent of frequency. The energy increase in each flutter motion cycle is examined using the work done by the generalized aerodynamic forces or by the self-excited forces along the bridge axis. Accordingly, their contribution to the aerodynamic damping can be clearly identified. The multimode flutter generation mechanism and the roles of flutter derivatives are investigated. Finally, the coupling effects on the buffeting response due to self-excited forces are also discussed.

INTRODUCTION

Flutter and buffeting responses are extremely important topics in the design of long-span bridges. For the construction of super long-span bridges with center spans of more than 2,000 m, it is recognized that the simple extrapolation of conventional technology does not satisfy the aerodynamic stability or economic feasibility requirements. New ideas regarding the structural modification and aerodynamic stabilization of the bridge deck section must be developed (Matsumoto et al. 1995; Diana et al. 1998). When investigating dynamic and aerodynamic stabilization strategies, it is very important to have an advanced understanding of the bridge aerodynamic behavior and the enhanced response prediction capability.

Numerous analytical investigations related to flutter and buffeting problems can be identified (e.g., Bleich 1948; Davenport 1962; Scanlan 1978a,b; Lin and Yang 1983; Xie and Xiang 1985; Miyata and Yamada 1988; Agar 1989; Matsumoto et al. 1994; Pfeil and Batista 1995; Matsumoto and Chen 1996; Jain et al. 1996; Katsuchi et al. 1999). Scanlan (1978a) proposed a basic theory for multimode flutter analysis. He also suggested a mode-by-mode approach based on the fact that practical flutter problems of long-span bridges are most likely damping-driven flutter and are dominated by the action of a single mode. Agar (1989) presented a modal technique in which complex eigenvalue problems are solved using an iterative procedure. Miyata et al. (1988) directly used the structural equations of physical coordinates for the complex eigenvalue computation without iterative calculations. However, this technique requires extensive computational effort. The state-space method without any iterative calculation was adopted in flutter analysis, flutter control system design, and buffeting analysis in the time domain (Xie and Xiang 1985; Matsumoto et al. 1994; Wilde and Fujino 1998). On the other hand, for the buffeting response analysis, the conventional mode-by-mode approach is widely used. Matsumoto et al. (1994) pointed out the importance of aerodynamic coupling among modes of vibration when estimating the buffeting response, particularly at higher wind velocities. They also proposed a time domain approach that involves frequency dependent characteristics of unsteady aerodynamic forces and aerodynamic coupling (Matsumoto and Chen 1996). The coupled flutter and buffeting problem has also been addressed by Jain et al. (1996) and Katsuchi et al. (1999).

Some analytical results of multimode flutter analyses of long-span bridges indicate that because of the closely spaced natural frequencies and the three-dimensional mode shapes, the aerodynamic coupling among modes becomes complicated. Furthermore, the coupled multimode flutter is not always initiated by the fundamental symmetric torsional mode (Miyata and Yamada 1988; Agar 1989). These results seem to be sensitive to the dynamic and aerodynamic characteristics of structures. The generation mechanism involved in multimode flutter behavior seems very complicated and has not yet been clearly classified. Although the aerodynamic coupling effects are considered in the flutter investigation, they are generally ignored when predicting the buffeting response. The contribution of aerodynamic coupling to the buffeting response that results from the changes in aerodynamic damping and modal coupling has also not been fully recognized in practice.

In this paper, the effects of aerodynamic coupling among modes of vibration on the flutter and buffeting responses of long-span bridges are examined. First, a frequency independent state-space equation is derived by describing the unsteady, self-excited aerodynamic forces in terms of rational functions. The effectiveness of the rational function approximation is demonstrated using a range of bluff body sections. The state-space format facilitates the multimode flutter analysis without iterative calculations. Next, aerodynamic coupling among modes is discussed in terms of the participation of natural modes in flutter motion, and more importantly, from the viewpoint of energy considerations regarding the work done by the self-excited forces. The multimode flutter generation mechanism and the roles of flutter derivatives are then investigated. Finally, the effects on the buffeting response of aerodynamic coupling due to the self-excited forces are also discussed.

EQUATION OF MOTION

The aerodynamic forces as shown in Fig. 1 are separated into their self-excited and buffeting components. The self-ex-

[1]Postdoctoral Res. Assoc., NatHaz Modeling Lab., Dept. of Civ. Engrg. and Geolog. Sci., Univ. of Notre Dame, Notre Dame, IN 46556.

[2]Prof., Dept. of Global Envir. Engrg., Kyoto Univ., Kyoto 606-8501, Japan.

[3]Prof. and Chair, Dept. of Civ. Engrg. and Geolog. Sci., Univ. of Notre Dame, Notre Dame, IN.

Note. Associate Editor: Apostolos S. Papageorgiou. Discussion open until June 1, 2000. To extend the closing date one month, a written request must be filed with the ASCE Manager of Journals. The manuscript for this paper was submitted for review and possible publication on February 2, 1999. This paper is part of the ***Journal of Engineering Mechanics***, Vol. 126, No. 1, January, 2000. ©ASCE, ISSN 0733-9399/00/0001-0017–0026/$8.00 + $.50 per page. Paper No. 20165.

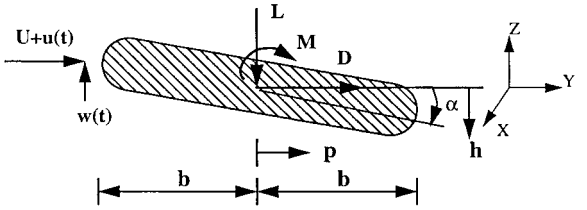

FIG. 1. Aerodynamic Forces on Bridge Deck

cited forces per unit span are expressed in the extended Scanlan's format below (Scanlan 1978a, 1993):

$$L_{se}(t) = \frac{1}{2}\rho U^2(2b)\left(kH_1^*\frac{\dot{h}}{U} + kH_2^*\frac{b\dot{\alpha}}{U} + k^2H_3^*\alpha + k^2H_4^*\frac{h}{b} + kH_5^*\frac{\dot{p}}{U} + k^2H_6^*\frac{p}{b}\right) \quad (1a)$$

$$D_{se}(t) = \frac{1}{2}\rho U^2(2b)\left(kP_1^*\frac{\dot{p}}{U} + kP_2^*\frac{b\dot{\alpha}}{U} + k^2P_3^*\alpha + k^2P_4^*\frac{p}{b} + kP_5^*\frac{\dot{h}}{U} + k^2P_6^*\frac{h}{b}\right) \quad (1b)$$

$$M_{se}(t) = \frac{1}{2}\rho U^2(2b^2)\left(kA_1^*\frac{\dot{h}}{U} + kA_2^*\frac{b\dot{\alpha}}{U} + k^2A_3^*\alpha + k^2A_4^*\frac{h}{b} + kA_5^*\frac{\dot{p}}{U} + k^2A_6^*\frac{p}{b}\right) \quad (1c)$$

where ρ = air density; U = mean wind velocity; $B = 2b$ = bridge deck width; $k = \omega b/U$ = reduced frequency; ω = circular frequency of vibration; h, p, and α = vertical, lateral, and torsional displacements, respectively; the over-dot denotes the partial differentiation with respect to time; and H_i^*, P_i^* and $A_i^*(i = 1 \sim 6)$ = flutter derivatives, which are functions of the reduced frequency and depend on the geometrical configuration of the bridge section and the approach flow.

For the bluff bridge deck sections, the flutter derivatives must be determined experimentally. This is done through a system identification method in the frequency or time domain using free vibration or forced vibration testing in a wind tunnel. The bridge deck section model is generally spring supported or driven in the vertical and/or torsional directions to identify the flutter derivatives H_i^* and $A_i^*(i = 1 \sim 4)$. The drag component and the components associated with lateral motion are generally negligible, but may become important for certain bridge deck configurations (Miyata et al. 1994). They can be identified through wind tunnel testing or simply by invoking the quasi-steady theory, as follows:

$$P_1^* = -\frac{2}{k}C_D, \quad P_2^* = -\frac{1}{2k}(C_D' - C_L), \quad P_3^* = \frac{1}{k^2}C_D',$$
$$P_5^* = \frac{1}{k}(C_D' - C_L), \quad H_5^* = \frac{2}{k}C_L, \quad A_5^* = -\frac{4}{k}C_M,$$
$$P_4^* = P_6^* = H_6^* = A_6^* = 0 \quad (2)$$

where C_L, C_D, and C_M = static lift, drag, and moment coefficients, respectively, and $C_D' = dC_D/d\alpha$.

The buffeting forces per unit span due to wind fluctuations are given by (Davenport 1962; Scanlan 1978b, 1993):

$$L_b(t) = -\frac{1}{2}\rho U^2 B\left[2C_{L\chi_{Lu}}\frac{u(t)}{U} + (C_L' + C_D)_{\chi_{Lw}}\frac{w(t)}{U}\right] \quad (3a)$$

$$D_b(t) = \frac{1}{2}\rho U^2 B\left[2C_{D\chi_{Du}}\frac{u(t)}{U} + C_{D\chi_{Dw}}'\frac{w(t)}{U}\right] \quad (3b)$$

$$M_b(t) = \frac{1}{2}\rho U^2 B^2\left[2C_{M\chi_{Mu}}\frac{u(t)}{U} + C_{M\chi_{Mw}}'\frac{w(t)}{U}\right] \quad (3c)$$

where χ_{Lu}, χ_{Lw}, χ_{Du}, χ_{Dw}, χ_{Mu}, and χ_{Mw} = aerodynamic admittance functions, which are functions of reduced frequency and dependent on the geometrical configuration of the bridge section; $C_L' = dC_L/d\alpha$ and $C_M' = dC_M/d\alpha$; and u and w = longitudinal and vertical wind velocity fluctuations, respectively.

The governing equation of dynamic motion of a bridge subjected to turbulent wind loads is expressed in terms of the generalized modal coordinates $\mathbf{q}$ as follows:

$$\mathbf{M}\ddot{\mathbf{q}} + \mathbf{C}\dot{\mathbf{q}} + \mathbf{K}\mathbf{q} = \mathbf{Q}_{se} + \mathbf{Q}_b \quad (4)$$

where $\mathbf{M}$, $\mathbf{C}$, and $\mathbf{K}$ = generalized mass, damping, and stiffness matrices, respectively; $\mathbf{Q}_{se}$ and $\mathbf{Q}_b$ = generalized self-excited and buffeting force vectors, respectively, and are expressed as

$$\mathbf{Q}_{se} = \frac{1}{2}\rho U^2\left(\mathbf{A}_s\mathbf{q} + \frac{b}{U}\mathbf{A}_d\dot{\mathbf{q}}\right) \quad (5)$$

$$\mathbf{Q}_b = \frac{1}{2}\rho U^2\left(\mathbf{A}_{bu}\frac{\mathbf{u}}{U} + \mathbf{A}_{bw}\frac{\mathbf{w}}{U}\right) \quad (6)$$

where $\mathbf{A}_s$ and $\mathbf{A}_d$ = aerodynamic stiffness and damping matrices, respectively, $\mathbf{A}_{bu}$ and $\mathbf{A}_{bw}$ = buffeting force matrices; and $\mathbf{u}$ and $\mathbf{w}$ = nodal fluctuating wind vectors for the u- and w- components, respectively. When calculating the buffeting forces, their spanwise correlations are taken into account through the joint acceptance functions.

MULTIMODE FLUTTER ANALYSIS

The above equation of motion can be expressed in the following state-space format:

$$\dot{\mathbf{Y}} = \mathbf{A}\mathbf{Y} + \mathbf{B}\mathbf{Q}_b \quad (7)$$

where

$$\mathbf{Y} = \begin{Bmatrix}\mathbf{q}\\ \dot{\mathbf{q}}\end{Bmatrix}, \quad \mathbf{A} = \begin{bmatrix}\mathbf{0} & \mathbf{I}\\ -\mathbf{M}^{-1}\mathbf{K}_1 & -\mathbf{M}^{-1}\mathbf{C}_1\end{bmatrix}, \quad \mathbf{B} = \begin{bmatrix}\mathbf{0}\\ \mathbf{M}^{-1}\end{bmatrix}$$
$$\mathbf{C}_1 = \mathbf{C} - \frac{1}{2}\rho U b\mathbf{A}_d \quad \mathbf{K}_1 = \mathbf{K} - \frac{1}{2}\rho U^2\mathbf{A}_s$$

The conventional way to solve this for the flutter problem is by omitting the buffeting forces and setting $\mathbf{q} = \mathbf{\Phi}e^{st}$ in the preceding equation. The solution of the complex eigenvalues and eigenvectors gives the modal frequencies, damping ratios, and modal shapes of the structure for a given wind velocity. These values differ from those of the natural modes because of the inclusion of the self-excited forces. Since the aerodynamic matrices $\mathbf{A}_s$ and $\mathbf{A}_d$ are functions of an unknown reduced frequency, the solution at any given wind velocity needs an iterative calculation for each eigenvalue until the assumed frequency used to evaluate the self-excited aerodynamic forces agrees with the imaginary part of the eigenvalue (Agar 1989).

Because of the closely spaced natural frequencies in the multimode analysis of long-span bridges, the target mode identification in the iterative calculation procedure must be done step-by-step, which may not permit full automation of the numerical procedure to realize the correct solution. This is time consuming and computationally cumbersome. An alternative way is to avoid iterative calculations by using a frequency independent state-space equation. This equation can be derived by expressing the self-excited forces as rational function approximations (Karpel 1982).

For the steady harmonic motion with circular frequency ω, i.e., $\mathbf{q}(t) = \mathbf{q}(i\omega)e^{i\omega t}$, the generalized self-excited forces are

$$\mathbf{Q}_{se}(t) = \mathbf{Q}(i\omega)e^{i\omega t} = \frac{1}{2}\rho U^2(\mathbf{A}_s + ik\mathbf{A}_d)q(i\omega)e^{i\omega t} \tag{8}$$

The matrices $\mathbf{A}_{sd}(ik) = \mathbf{A}_s + ik\mathbf{A}_d$ can be expressed in terms of rational function approximation as

$$\mathbf{A}_{sd}(ik) = \mathbf{A}_1 + \mathbf{A}_2(ik) + \mathbf{A}_3(ik)^2 + \sum_{l=1}^{m} \frac{\mathbf{A}_{l+3}ik}{ik + d_l} \tag{9}$$

where matrix $\mathbf{A}_1$, $\mathbf{A}_2$, $\mathbf{A}_3$, $\mathbf{A}_{l+3}$ and d_l ($d_l \geq 0$; $l = 1 \sim m$) are frequency-independent coefficients. The $\mathbf{A}_1$ and $\mathbf{A}_2$ terms are the noncirculatory static-aerodynamics and aerodynamic damping, respectively; The $\mathbf{A}_3$ term is the additional aerodynamic mass due to the wind loads and is generally negligible. The rational partial fractions represent unsteady characteristics of the self-excited forces in terms of transfer functions in which the aerodynamic forces lag the velocity components and permit approximations of the time delays by the positive parameter d_l ($l = 1 \sim m$). This approximation can be identified by linear and nonlinear optimization in a least-squares sense to approximate the experimentally obtained tabular data of the aerodynamic matrix $\mathbf{A}_{sd}$, which is defined at specified values of reduced frequencies k_n ($n = 1, 2, \ldots$).

Employing the concept of analytic continuation in the region near the imaginary axis of the complex plane (i.e., with small positive or negative damping), the rational function approximations of the self-excited forces can be extended to arbitrary motion $\mathbf{q}(t) = \mathbf{q}(s)e^{st}$ as

$$\begin{aligned}\mathbf{Q}_{se}(t) &= \frac{1}{2}\rho U^2\left(\mathbf{A}_1 + \mathbf{A}_2\frac{sb}{U} + \mathbf{A}_3\left(\frac{sb}{U}\right)^2 + \sum_{l=1}^{m}\frac{\mathbf{A}_{l+3}sb/U}{sb/U + d_l}\right)\mathbf{q}(s)e^{st} \\ &= \frac{1}{2}\rho U^2\left(\mathbf{A}_1\mathbf{q} + \mathbf{A}_2\frac{b}{U}\dot{\mathbf{q}} + \mathbf{A}_3\left(\frac{b}{U}\right)^2\ddot{\mathbf{q}} + \sum_{l=1}^{m}\mathbf{q}_{sel}\right)\end{aligned} \tag{10}$$

where $s = (-\xi + i)\omega$; ξ = critical damping ratio; and $\mathbf{q}_{sel}$ ($l = 1 \sim m$) are additional vectors representing the unsteady aerodynamic states, and are given by

$$\dot{\mathbf{q}}_{sel} = -\frac{U}{b}d_l\mathbf{q}_{sel} + \mathbf{A}_{l+3}\dot{\mathbf{q}} \quad (l = 1 \sim m) \tag{11}$$

It is noted that there is a slight difference between the descriptions of the self-excited forces for arbitrary motion in (5) and (10), which reflects the influence of the damping ratio. Matrices $\mathbf{A}_s$ and $\mathbf{A}_d$ in (5) are functions only of the reduced frequency, but the corresponding matrices defined in (10) are also influenced by the damping ratio. Although the effect of the damping ratio on the self-excited forces is a question open for discussion, it will be illustrated in the following part of this paper that for a general damping level, this difference is negligible for the analysis of flutter and buffeting responses.

Substituting (10) and (11) into (4) and expressing it in the state-space form gives

$$\dot{\bar{\mathbf{Y}}} = \bar{\mathbf{A}}\bar{\mathbf{Y}} + \bar{\mathbf{B}}\bar{\mathbf{Q}}_b \tag{12}$$

where

$$\bar{\mathbf{Y}} = \begin{Bmatrix}\mathbf{q}\\ \dot{\mathbf{q}}\\ \mathbf{q}_{se1}\\ \vdots\\ \mathbf{q}_{sem}\end{Bmatrix},$$

$$\bar{\mathbf{A}} = \begin{bmatrix}\mathbf{0} & \mathbf{I} & \mathbf{0} & \cdots & \mathbf{0}\\ -\bar{\mathbf{M}}^{-1}\bar{\mathbf{K}} & -\bar{\mathbf{M}}^{-1}\bar{\mathbf{C}} & \frac{1}{2}\rho U^2\bar{\mathbf{M}}^{-1} & \cdots & \frac{1}{2}\rho U^2\bar{\mathbf{M}}^{-1}\\ \mathbf{0} & \mathbf{A}_4 & -\frac{U}{b}d_1\mathbf{I} & \cdots & \mathbf{0}\\ \vdots & \vdots & \vdots & & \vdots\\ \mathbf{0} & \mathbf{A}_{3+m} & \mathbf{0} & \cdots & -\frac{U}{b}d_m\mathbf{I}\end{bmatrix},$$

$$\bar{\mathbf{B}} = \begin{bmatrix}\mathbf{0}\\ \bar{\mathbf{M}}^{-1}\\ \mathbf{0}\\ \vdots\\ \mathbf{0}\end{bmatrix}$$

and

$$\bar{\mathbf{M}} = \mathbf{M} - \frac{1}{2}\rho b^2\mathbf{A}_3, \quad \bar{\mathbf{C}} = \mathbf{C} - \frac{1}{2}\rho Ub\mathbf{A}_2, \quad \bar{\mathbf{K}} = \mathbf{K} - \frac{1}{2}\rho U^2\mathbf{A}_1$$

Since the preceding equation is linear and frequency independent, it has convenient applications to various simulation and optimization procedures and modern control design techniques. This method is also used for analyzing the dynamic response of systems with frequency-dependent parameters in the time domain. Similar applications can be found in the interactions of the structures with such continuous media as soils and fluids (Spanos and Zeldin 1997). In bridge aerodynamics, the flutter and buffeting response can be calculated in the time domain by the same numerical formulation. In addition, the unsteady self-excited forces and aerodynamic coupling effects among natural modes can be readily taken into account (Matsumoto et al. 1994; Matsumoto and Chen 1996). The main advantage of applying this approach in multimode flutter analysis is that all eigenvalues corresponding to the natural modes of the structure and all unsteady aerodynamic states at a given wind velocity can be computed without iterative calculations.

At a given wind velocity, the eigenvalue and the eigenvector of a prescribed complex mode can be expressed as

$$s = (-\xi + i)\omega; \quad \mathbf{\Phi} = \mathbf{a} + i\mathbf{b} \tag{13a,b}$$

Because of aerodynamic coupling, the mode shapes are coupled. For the sake of illustration, the terms ''mode branch'' is assigned to identify all the complex modes that emerge from a natural mode due to aerodynamic effects as the wind velocity increases. In a prescribed mode branch, the magnitude and phase of the kth natural mode are given as

$$|\Phi|_k = \sqrt{a_k^2 + b_k^2}; \quad \varphi_k = \tan^{-1}(b_k/a_k) \tag{14a,b}$$

The system is stable when all of the eigenvalues lie to the left of the imaginary axis in the complex plane. The onset of flutter occurs when one of the eigenvalues has a zero real part, which indicates that the damping is zero. The mode branch in which flutter takes place is also referred to here as the flutter mode branch.

At the critical flutter velocity, the generalized modal coordinate $\mathbf{q}(t)$ and the nodal displacement are expressed by the complex flutter mode as

$$\mathbf{q}(t) = \{|\Phi|_i \sin(\omega t + \varphi_i)\} \tag{15}$$

$$r(x, t) = \sum_{i=1}^{N} r_i(x)|\Phi|_i \sin(\omega t + \varphi_i) = r_0(x)\sin(\omega t + \varphi_r(x)) \tag{16}$$

where r indicates the symbols of h, p, and α; $r_0(x)$ and $\varphi_r(x)$ = amplitude and phase of $r(x, t)$; $r_i(x)$ represents the natural mode shape in ith mode; N = mode number; and x = coordi-

nate of the section along the bridge axis. It is clear that the coupled flutter motion is three-dimensional and that the phase shift exists among different response components.

To improve our understanding of the multimode flutter generation mechanism, it is important to clarify the effects of aerodynamic coupling among modes in terms of both the participation of the natural modes in the flutter motion and the contribution to the system damping. Clarification of the work distribution done by the aerodynamic forces along the bridge axis will also be useful for the delineating efficient structural and/or aerodynamic flutter suppression strategies.

The increase in energy per flutter motion cycle, ΔE, can be expressed by the work done by the generalized aerodynamic forces as (excluding the contribution of the structural damping force)

$$\Delta E = \int_0^{2\pi/\omega} \frac{1}{2}\rho U^2 \left(\dot{\mathbf{q}}^T\mathbf{A}_s\mathbf{q} + \frac{b}{U}\dot{\mathbf{q}}^T\mathbf{A}_d\dot{\mathbf{q}}\right) dt = \sum_{i=1}^{N}\sum_{j=1}^{N} (\Delta E_{d_{ij}} + \Delta E_{s_{ij}}) \tag{17}$$

where $\Delta E_{d_{ij}}$ and $\Delta E_{s_{ij}}$ indicate the contribution of the aerodynamic damping coupling and stiffness coupling between the ith and jth modes, respectively, and are expressed as

$$\Delta E_{d_{ij}} = \Delta E_{d_{ji}} = \frac{1}{4}\rho U^2 \pi |\Phi|_i |\Phi|_j (A_{d_{ij}} + A_{d_{ji}}) k \cos(\varphi_i - \varphi_j) \tag{18}$$

$$\Delta E_{s_{ij}} = \Delta E_{s_{ji}} = -\frac{1}{4}\rho U^2 \pi |\Phi|_i |\Phi|_j (A_{s_{ij}} + A_{s_{ji}}) \sin(\varphi_i - \varphi_j) \tag{19}$$

The total potential energy of the system can be expressed as

$$E = \sum_{i}^{N}\sum_{j}^{N} |\Phi|_i |\Phi|_j \left(K_{ij} - \frac{1}{2}\rho U^2 A_{s_{ij}}\right) \cos(\varphi_i - \varphi_j) \tag{20}$$

Accordingly, the logarithmic aerodynamic damping ratio is given by

$$\delta = 2\pi\xi = -\Delta E/(2E) = \sum_{i=1}^{N}\sum_{j=1}^{N} (\delta_{d_{ij}} + \delta_{s_{ij}}) \tag{21}$$

$$\delta_{d_{ij}} = \delta_{d_{ji}} = -\Delta E_{d_{ij}}/(2E); \quad \delta_{s_{ij}} = \delta_{s_{ji}} = -\Delta E_{s_{ij}}/(2E) \tag{22a,b}$$

where $\delta_{d_{ij}}$, $\delta_{s_{ij}}$ = contribution to the aerodynamic damping due to aerodynamic damping coupling and stiffness coupling between the ith and jth modes.

The increase in energy of the bridge per cycle of flutter motion can be further expressed in terms of the work done by the self-excited forces:

$$\Delta E = W_{Lse} + W_{Dse} + W_{Mse} = \int_{span}\int_0^{2\pi/\omega} (L_{se}\dot{h} + D_{se}\dot{p} + M_{se}\dot{\alpha})\, dt\, dx \tag{23}$$

where, for example

$$W_{L_{se}} = W_{L_{seh}} + W_{L_{sep}} + W_{L_{se\alpha}} = \int_{span}\int_0^{2\pi/\omega} (L_{seh} + L_{sep} + L_{se\alpha})\dot{h}\, dt\, dx \tag{24}$$

$$W_{L_{se\alpha}} = \int_{span}\int_0^{2\pi/\omega} L_{se\alpha}\dot{h}\, dt\, dx = \int_{span}\int_0^{2\pi/\omega} \frac{1}{2}\rho U^2(2b)\left(kH_2^*\frac{b\dot{\alpha}}{U} + k^2H_3^*\alpha\right)\dot{h}\, dt\, dx = \pi\rho b^3\omega^2 \int_{span} h_0(x)\alpha_0(x)[H_2^*\cos(\varphi_\alpha - \varphi_h) + H_3^*\sin(\varphi_\alpha - \varphi_h)]\, dx \tag{25}$$

where $W_{L_{se\alpha}}$ indicates the work done by the lift component due to torsional motion, with analogous definitions for the other components. The corresponding contribution to the system damping is

$$\delta_{L_{se\alpha}} = -W_{L_{se\alpha}}/(2E) \tag{26}$$

From the preceding equations, the contribution of aerodynamic coupling among modes to the system damping, and the exciting or damping roles of each self-excited force component along the bridge axis, can be identified. These effects depend on the modal characteristics and the flutter derivatives of the bridge

BUFFETING RESPONSE ANALYSIS

The power spectral density (PSD) matrices of the vectors of generalized modal response $\mathbf{q}$ and nodal displacement $\mathbf{Z} = \boldsymbol{\Psi}\mathbf{q}$ are given by

$$\mathbf{S}_\mathbf{q}(\omega) = \mathbf{H}^*(\omega)\mathbf{S}_{\mathbf{Q}_b}(\omega)\mathbf{H}(\omega)^T \tag{27}$$

$$\mathbf{S}_\mathbf{Z}(\omega) = \boldsymbol{\Psi}\mathbf{H}^*(\omega)\mathbf{S}_{\mathbf{Q}_b}(\omega)\mathbf{H}(\omega)^T\boldsymbol{\Psi}^T \tag{28}$$

where $\boldsymbol{\Psi}$ = mode shape matrix, and $\mathbf{H}(\omega)$ = transfer function matrix.

$$\mathbf{H}(\omega) = \left(-\omega^2\mathbf{M} + i\omega\left(\mathbf{C} - \frac{1}{2}\rho U b\mathbf{A}_d\right) + \mathbf{K} - \frac{1}{2}\rho U^2\mathbf{A}_s\right)^{-1} \tag{29}$$

and subscripts * and T denote the complex conjugate and transpose, respectively.

Because of the aerodynamic coupling among modes of vibration, the off-diagonal components of matrix $\mathbf{H}(\omega)$ generally have nonzero values depending on the dynamic and aerodynamic characteristics of the bridge. These components may strongly influence the buffeting response as the wind velocity increases.

The PSD matrix of the generalized buffeting forces is given by:

$$\mathbf{S}_{\mathbf{Q}_b} = \frac{1}{4}\rho^2 U^2(\mathbf{A}_{bu}^*\mathbf{S}_{uu}\mathbf{A}_{bu}^T + \mathbf{A}_{bu}^*\mathbf{S}_{uw}\mathbf{A}_{bw}^T + \mathbf{A}_{bw}^*\mathbf{S}_{wu}\mathbf{A}_{bu}^T + \mathbf{A}_{bw}^*\mathbf{S}_{ww}\mathbf{A}_{bw}^T) \tag{30}$$

where $\mathbf{S}_{uu}$ and $\mathbf{S}_{ww}$ = PSD matrices of the $\mathbf{u}$ and $\mathbf{w}$ components, respectively, and $\mathbf{S}_{uw} = \mathbf{S}_{wu}^*$ = cross-spectral density (CSD) matrix between the $\mathbf{u}$ and $\mathbf{w}$ components and is generally negligible.

The PSD components of the $\mathbf{u}$ and $\mathbf{w}$ vectors used herein are given by the von Kármán spectra as follows. Other expressions for their quantities can also be used

$$\frac{fS_{u_iu_i}(f)}{\sigma_u^2} = \frac{4(fL_u^y/U)}{(1 + 70.78(fL_u^y/U)^2)^{5/6}} \tag{31a}$$

$$\frac{fS_{w_iw_i}(f)}{\sigma_w^2} = 2(fL_w^y/U)\frac{1 + 188.8fL_w^y/U)^2}{(1 + 70.78(fL_w^y/U)^2)^{11/6}} \tag{31b}$$

The CSD components are given as

$$S_{r_i r_j}(f) = \sqrt{S_{r_i r_i}(f) S_{r_j r_j}(f)} \exp\left(-\lambda_r \frac{\eta_r}{2\pi}\right) \tag{32a}$$

$$\eta_r = \frac{0.747|x_i - x_j|}{L_r^x} \sqrt{1 + 70.78\left(\frac{f L_r^x}{U}\right)^2} \tag{32b}$$

where r indicates the symbols of u and w; L_r^x and L_r^y = integral scales of the r component in the across-wind and along-wind directions, respectively; σ_r and λ_r = standard deviation and decay factor of the coherence of the r component; x_i and x_j = coordinates of point i and j in across-wind direction; and $\omega = 2\pi f$.

The components of the $S_{\mathbf{q}}$ and $\mathbf{S_Z}$ matrices can be expressed as

$$S_{q_{ij}}(\omega) = \sum_{k=1}^{N} \sum_{l=1}^{N} H_{ik}^*(\omega) S_{Qb_{kl}}(\omega) H_{jl}(\omega) \tag{33}$$

$$S_{Z_i}(\omega) = \sum_{k=1}^{N} \sum_{l=1}^{N} \Psi_{ik} S_{q_{kl}}(\omega) \Psi_{il} \tag{34}$$

When the CSD between different generalized buffeting forces are negligible in comparison with the PSD $S_{Qb_{ii}}(\omega)$, i.e., $S_{Qb_{ij}}(\omega) = 0$ $(i \neq j)$, the component of $\mathbf{S_q}(\omega)$ becomes

$$S_{q_{ij}}(\omega) = \sum_{k=1}^{N} H_{ik}^*(\omega) S_{Qb_{kk}}(\omega) H_{jk}(\omega) \tag{35}$$

When the aerodynamic coupling among modes is neglected, i.e., $H_{ij}(\omega) = 0$ $(i \neq j)$, $S_{q_{ij}}(\omega)$ is then given as

$$S_{q_{ij}}(i\omega) = H_{ii}^*(\omega) S_{Qb_{ij}}(\omega) H_{jj}(\omega) \tag{36}$$

When both $S_{Qb_{ij}}(\omega)$ and $H_{ij}(\omega)$ $(i \neq j)$ are neglected, it becomes the following expressions, used in the conventional mode-by-mode approach:

$$S_{q_{ii}}(\omega) = |H_{ii}(\omega)|^2 S_{Qb_{ii}}(\omega); \quad S_{q_{ij}}(\omega) = 0 \quad (i \neq j) \tag{37a,b}$$

The standard deviations are given by

$$\sigma_{q_{ii}}^2 = \int_0^\infty S_{q_{ii}}(i\omega)\, d\omega; \quad \sigma_{Z_i}^2 = \int_0^\infty S_{Z_i}(i\omega)\, d\omega \tag{38a,b}$$

EXAMPLE

A long-span suspension bridge with a center span of nearly 2,000 m is used to illustrate the multimode flutter and buffeting response analysis. The logarithmic structural damping ratio for each mode is assumed to be 0.02. Details concerning other structural parameters are omitted for brevity. To simplify discussion of the fundamental characteristics of the flutter and buffeting response, only the aerodynamic forces acting on the bridge deck are involved. The aerodynamic parameters are assumed to be uniform along the bridge axis, and the variations due to static rotation are ignored. The bridge deck used in this study is a typical streamlined section. The static coefficients of the deck section are $C_D = 0.3230$, $dC_D/d\alpha = 0$, $C_L = 0.0942$, $dC_L/d\alpha = 1.905$, and $C_M = 0.0104$, $dC_M/d\alpha = 0.2717$. The flutter derivatives $H_1^* \sim H_4^*$ and $A_1^* \sim A_4^*$ are evaluated using the Theodorsen function. The other flutter derivatives $P_1^* \sim P_6^*$, A_5^*, A_6^*, H_5^*, and H_6^*, are calculated by the quasi-steady theory. The terms χ_{Du}, χ_{Dw} are given by Davenport (1962) with a decay factor of 8, and χ_{Lu}, χ_{Lw}, χ_{Mu}, χ_{Mw} are given by the Sears function. The spanwise correlations of buffeting forces are assumed to be identical to the wind fluctuations. The mean wind velocity is normal to the bridge axis, and $\sigma_u/U = 10\%$, $\sigma_w/U = 5\%$, $L_u^x = L_u^y = 80$ m, $L_w^x = L_w^y = 40$ m, and $\lambda_u = \lambda_w = 8$. In addition, a rectangular cross section with an aspect ratio $B/D = 10$ (B: body width; D: body depth) is also considered in the flutter analysis for comparison. For this section, the flutter derivatives $H_1^* \sim H_4^*$ and $A_1^* \sim A_4^*$ are determined experimentally (Matsumoto et al. 1995), and other dynamic and aerodynamic parameters are assumed to be the same as those used in the earlier example.

Rational Function Approximation

To illustrate the effectiveness of the rational function approximation of unsteady aerodynamic forces, a two-dimensional section model system with vertical and torsional degrees of freedom is considered here as an example. It can easily be extended to multimode flutter calculation.

The self-excited forces are expressed in the following matrix form:

$$\begin{bmatrix} L_{se} \\ M_{se} \end{bmatrix} = \frac{1}{2}\rho U^2 \begin{bmatrix} 2b & 0 \\ 0 & 2b^2 \end{bmatrix} \cdot \begin{bmatrix} k^2(H_4^* + iH_1^*) & k^2(H_3^* + iH_2^*) \\ k^2(A_4^* + iA_1^*) & k^2(A_3^* + iA_2^*) \end{bmatrix} \begin{bmatrix} h/b \\ \alpha \end{bmatrix} \tag{39}$$

and the flutter derivative matrix is expressed in terms of the rational function as

$$\begin{bmatrix} k^2(H_4^* + iH_1^*) & k^2(H_3^* + iH_2^*) \\ k^2(A_4^* + iA_1^*) & k^2(A_3^* + iA_2^*) \end{bmatrix} = \mathbf{A}_1 + \mathbf{A}_2(ik) + \mathbf{A}_3(ik)^2 + \sum_{l=1}^{m} \frac{\mathbf{A}_{l+3} ik}{ik + d_l} \tag{40}$$

Figs. 2 and 3 show the flutter derivatives A_2^* and A_3^* for rectangular cross sections with aspect ratios of $B/D = 5$, 10,

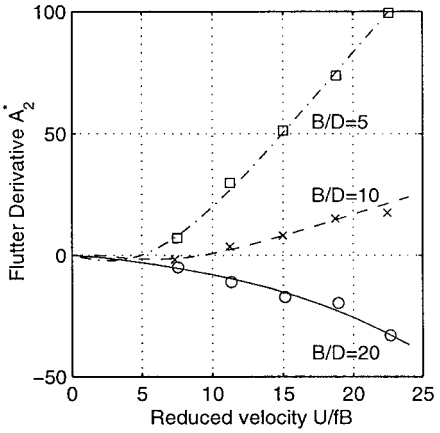

FIG. 2. Rational Function Approximation of A_2^* for Rectangular Cross Sections

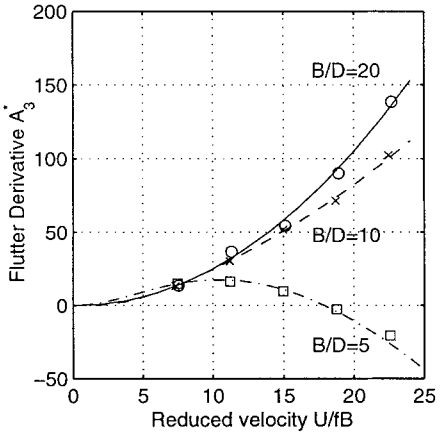

FIG. 3. Rational Function Approximation of A_3^* for Rectangular Cross Sections

and 20. The experimental data points (Matsumoto et al. 1995) are denoted by square, cross, and circle dots for B/D = 5, 10, and 20, respectively. The rational functions for these sections that have two lag terms are determined by linear and nonlinear optimization and are represented by a dashed dotted line, a dashed line, and a solid line, respectively. The results indicate that the unsteady, self-excited aerodynamic forces can be represented by the rational functions with good accuracy.

Flutter Analysis

In order to illustrate the influence of the different descriptions of the self-excited forces for arbitrary motion as expressed in (5) and (10), the changes in the frequencies and damping ratios with wind velocity are compared as shown in Fig. 4 for the bridge with a streamlined section. The circles and solid lines represent the results using the frequency-dependent state-space equation (7) and the frequency-independent state-space equation (12), respectively. In these analyses, only the fundamental symmetric vertical and torsional modes (i.e., mode 2 and mode 10), the second and third symmetric vertical modes (i.e., mode 8 and mode 11) are considered. The results are in very good agreement and indicate that the difference in the descriptions of the self-excited forces is negligible for the response analysis.

Various natural-mode combinations are used in the calculation to investigate the natural-mode participation in the multimode flutter of the bridge with a streamlined deck section. Figs. 5 and 6 show the variation of frequencies and damping ratios with wind velocity corresponding to complex mode shapes. In the cases without the lateral symmetric mode (i.e., mode 9), the damping of the branch developed from the fundamental symmetric torsional mode becomes negative past the flutter onset velocity. It is noted that higher vertical modes (e.g., mode 8 and 11) do not significantly influence the flutter conditions. Nevertheless, when mode 9 is included in the analysis, the flutter is initiated from this mode branch, although the onset velocity is almost the same as that without this mode. Above approximately 60 m/s, the frequency and damping of mode 9 branch change with wind velocity along almost the same path as mode 10 branch followed when mode 9 was not included. From the magnitude of each natural mode included in the mode 9 and mode 10 branches (Table 1), it is noted that the torsional mode 10 dominates the mode 9 branch beyond the flutter onset velocity (68.9 m/s). Fig. 7 shows the amplitude of the vertical, lateral, and torsional displacements along

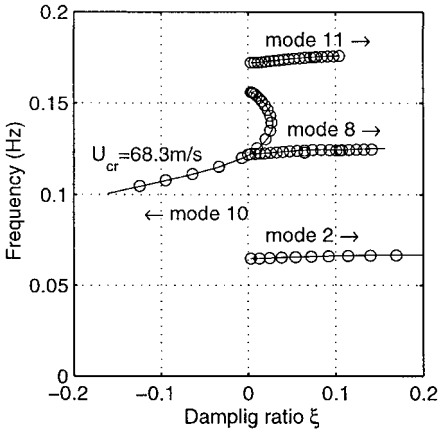

FIG. 4. Comparison for Different Descriptions of Self-Excited Forces

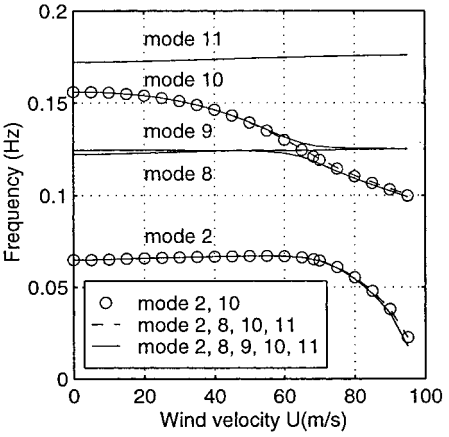

FIG. 5. Frequency versus Wind Velocity (Streamlined Section)

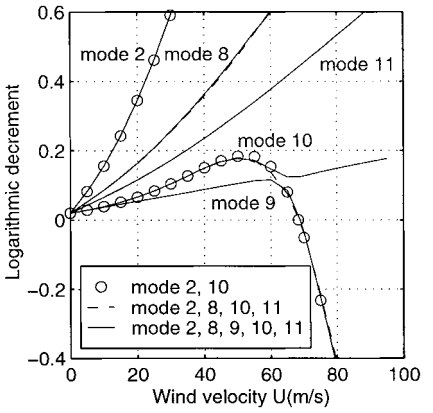

FIG. 6. Damping Ratio versus Wind Velocity (Streamlined Section)

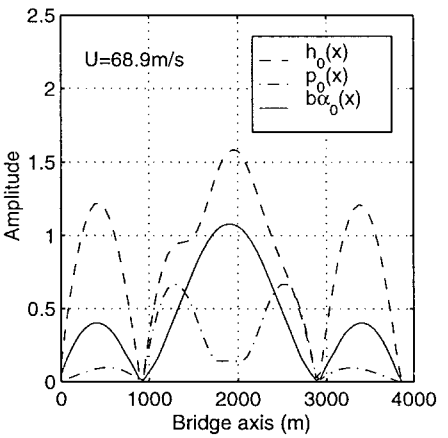

FIG. 7. Amplitude of Coupled Flutter Motion along Bridge Axis (Streamlined Section)

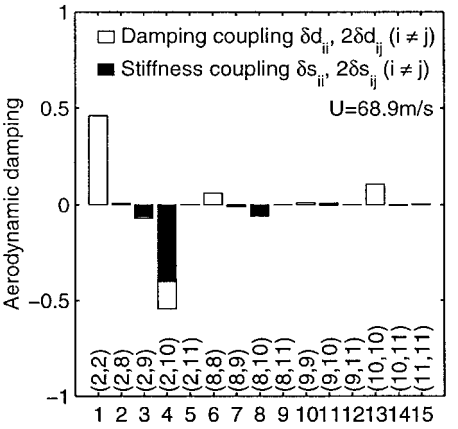

FIG. 8. Aerodynamic Damping due to Aerodynamic Coupling among Modes (Streamlined Section)

the bridge axis in flutter motion. Since only the amplitude is presented here, it should be noted that a phase shift exists between response components.

Fig. 8 presents aerodynamic damping due to stiffness coupling and damping coupling among modes. The sum of all components equals the aerodynamic damping of the bridge. It is obvious that the aerodynamic coupling between mode 2 and mode 10—in particular, the stiffness-coupling corresponding to the flutter derivatives H_3^*—produces negative damping and contributes strongly to the occurrence of flutter. Mode 9 has only marginal influence on flutter. The analysis consisting of the first fifteen modes was also conducted and gave the flutter onset velocity as 69.3 m/s, which is very close to the result given by the two-mode case (mode 2 and mode 10). It can be concluded in most cases that the fundamental vertical and torsional modes are the dominant modes for the multimode flutter. Their aerodynamic coupling, induced by the coupled self-excited forces, drives the system with negative damping past the flutter onset velocity.

Fig. 9 indicates the contribution of the work done by the aerodynamic forces along the bridge axis to the system damping. The sum of all components along the bridge axis equals the aerodynamic damping of the bridge. It can be seen that the coupled self-excited forces $L_{se\alpha}$ and M_{seh}, i.e., the lift inducted by the torsional motion and the moment induced by the vertical motion acting on the center span, are the main source of introducing negative damping to the bridge. Therefore, for the purpose of improving the coupled flutter stability, it is important to reduce the coupled self-excited forces and the aerodynamic stiffness by modifying the configuration of the bridge deck section and/or to reduce the structural coupling by modifying the dynamic characteristics.

Since the changes in deck shape and structural parameters do not affect the sign of the phase shift between vertical and torsional motions in the coupled flutter motion, and do not affect the sign of the flutter derivatives (except for A_2^* for relatively bluff sections and H_2^* that may show very small negative values, as in the case of airfoil), the conclusions related to the effects of aerodynamic coupling on the coupled flutter are valid for most bridges.

Figs. 10 and 11 show the results of the bridge with a rectangular deck section with an aspect ratio of $B/D = 10$. In this case, since the A_2^* associated with torsional aerodynamic damping changes from a negative value to a positive one as the wind velocity increases, the damping driven flutter occurs at the onset velocity of 48.8 m/s when only the single torsional mode is considered. However, the coupling between the vertical and torsional modes also introduces negative damping and thus reduces the onset velocity to 40.7 m/s when the vertical mode is included in the analysis (Fig. 11). However, the coupled vertical motion is much smaller than that of the streamlined deck section (Fig. 12).

Figs. 13 and 14 indicate that the coupled forces $L_{se\alpha}$ and M_{seh}, particularly the damping coupling terms corresponding to the flutter derivatives A_1^* and H_2^*, provide negative aerodynamic damping. Because the sign of the phase shift between the vertical and torsional motions is opposite to that of the streamlined section, the stiffness coupling shows a stabilizing effect in this case. Fig. 15 shows the aerodynamic damping due to the work done by the self-excited forces at a wind velocity of 50 m/s. Along with $L_{se\alpha}$ and M_{seh}, $M_{se\alpha}$ also produces negative damping because of the positive value of A_2^*. It is obvious that even when a single-mode flutter would occur at a given wind velocity, the coupling effects may result in a

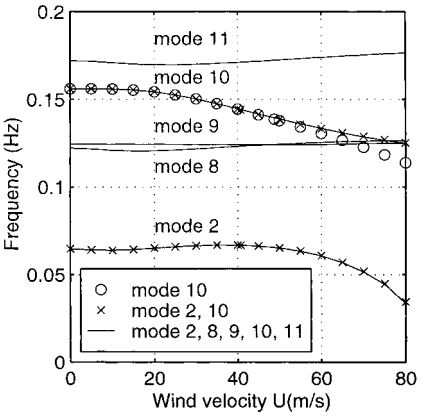

FIG. 10. Frequency versus Wind Velocity (Rectangular Section)

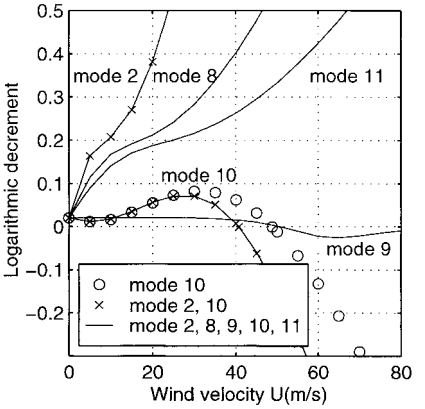

FIG. 11. Damping Ratio versus Wind Velocity (Rectangular Section

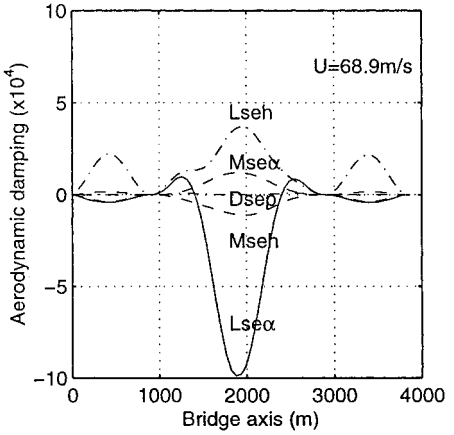

FIG. 9. Aerodynamic Damping due to Work Done by Self-Excited Forces (Streamlined Section)

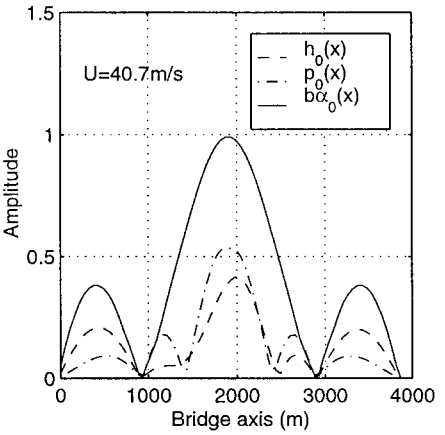

FIG. 12. Amplitude of Coupled Flutter Motion along Bridge Axis (Rectangular Section)

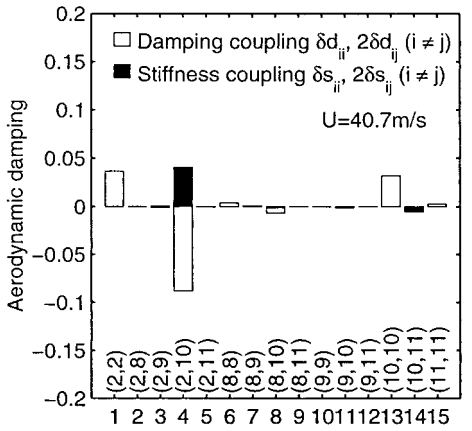

FIG. 13. Aerodynamic Damping due to Aerodynamic Coupling among Modes (Rectangular Section)

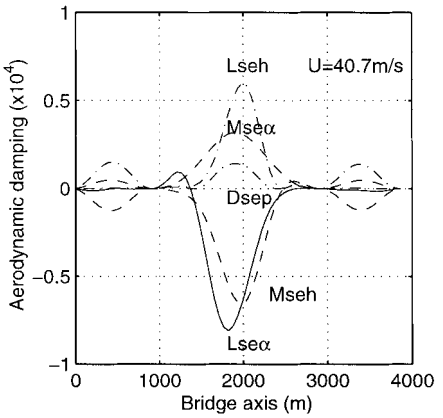

FIG. 14. Aerodynamic Damping due to Work Done by Self-Excited Forces (Rectangular Section)

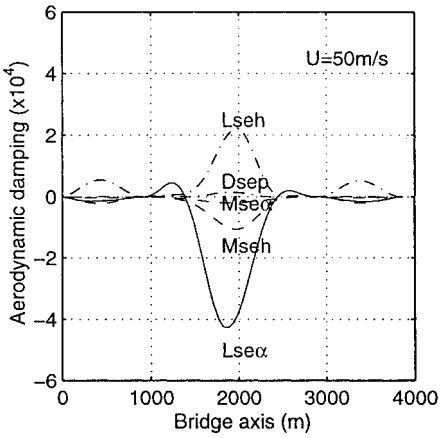

FIG. 15. Aerodynamic Damping due to Work Done by Self-Excited Forces (Rectangular Section)

lower flutter onset velocity. Similar results have been illustrated in wind tunnel testing for two-dimensional *H*-shaped sections (Karman and Dann 1949). In such a case, the mode-by-mode analysis approach would lead to nonconservative results for the onset wind velocity prediction, as compared to the multimode method.

Buffeting Analysis

The first 15 natural modes are considered in the buffeting response analysis. Fig. 16 indicates the influence of aerodynamic coupling among modes on the modal damping as the mean wind velocity increases. The solid lines and dashed lines are the results with and without coupling, respectively. There are some significant differences noted at higher wind velocities, particularly in the vertical and torsional coupled mode branch. Fig. 17 shows the transfer functions between the generalized modal forces and the generalized modal response coordinates such as $H_{2,2}$ and $H_{2,10}$ at a range of wind velocities (e.g., $H_{2,10}$ represents the transfer function between the generalized modal force in the tenth mode and the generalized modal displacement in the second mode). The dashed line also gives the results without the aerodynamic coupling at a mean wind velocity of 60 m/s. It can be seen that the term $H_{2,2}$ also consists of a component from the torsional mode branch at the torsional mode frequency due to aerodynamic coupling. The term $H_{2,10}$, which is always ignored in the conventional method

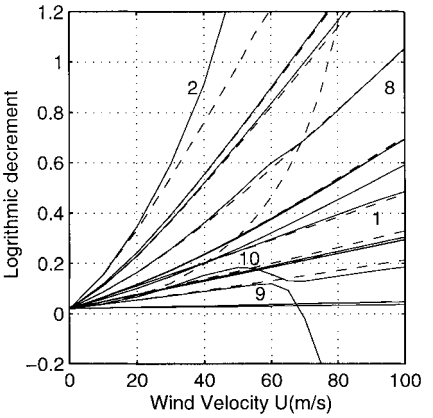

FIG. 16. Damping Ratio versus Wind Velocity (—— with Coupling; – – – – w/o Coupling)

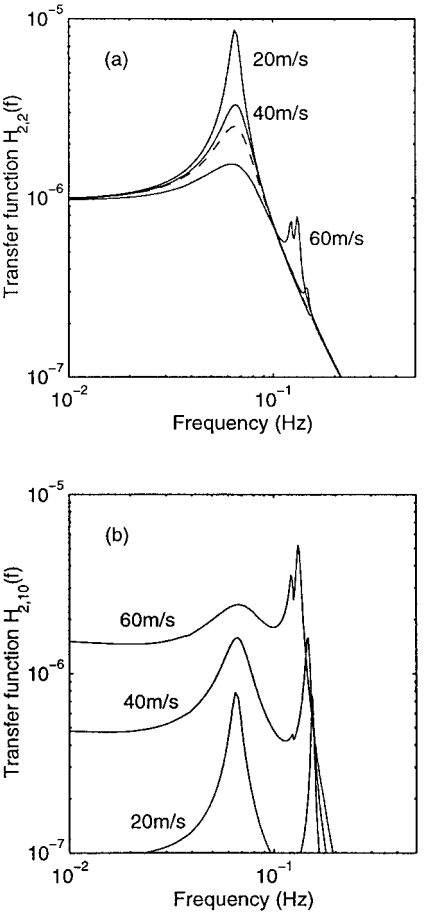

FIG. 17. Transfer Functions of Modal Responses

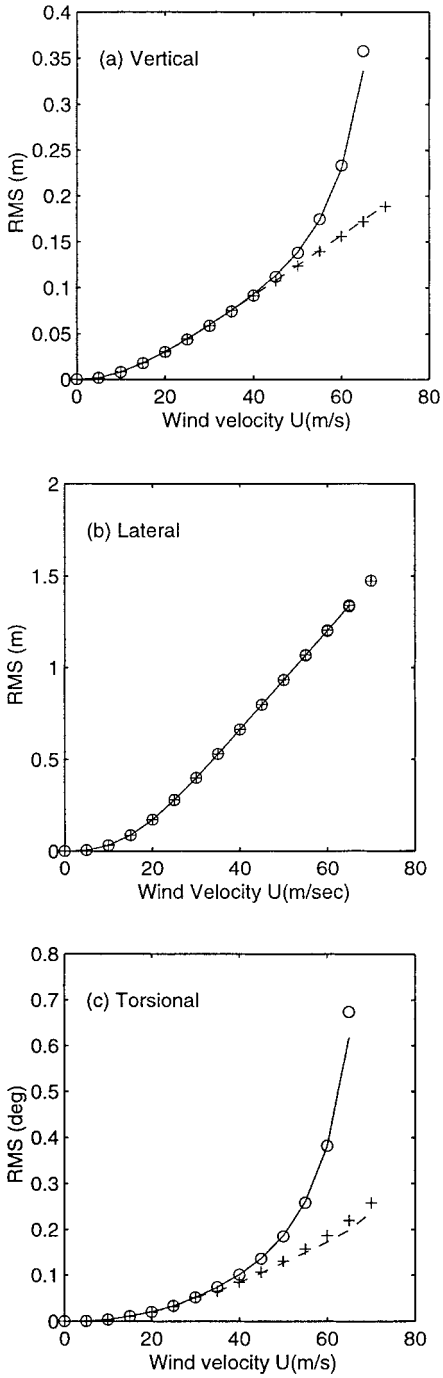

FIG. 18. RMS of Responses at Center of Main Span

without the aerodynamic coupling, cannot be neglected at higher wind velocities.

The RMS values of the displacement at the main span center are shown in Fig. 18. The solid lines and the dashed lines indicate the results with (33) and without (36) aerodynamic coupling, respectively, including the CSD of the generalized buffeting forces, $S_{Qb_{ij}}(\omega)$ ($i \neq j$; i, j: mode number). Circles and crosses represent the results with (35) and without (37) aerodynamic coupling, respectively, excluding $S_{Qb_{ij}}(\omega)$ ($i \neq j$; i, j: mode number). It is obvious that the aerodynamic coupling strongly affects the buffeting response due to self-excited aerodynamic forces at higher wind velocities, and that the buffeting response will be underestimated using the conventional mode-by-mode analysis approach. The results also suggest that omission of the CSD between different generalized buffeting forces in the analysis does not significantly influence the response predictions.

CONCLUDING REMARKS

A frequency-independent state-space equation is derived to represent the equation of motion by expressing the self-excited forces in terms of rational function approximations. This format is used for flutter analysis by solving the complex eigenvalue problem to determine the frequencies, damping ratios, and mode shapes at different wind velocities. This approach does not need any iterative calculation. Therefore, the identification of a target mode at each step for each mode branch calculation, as needed in the conventional approach, can be avoided to promote computational efficiency.

The aerodynamic coupling among modes and its damping or exciting roles are investigated from the viewpoint of system energy in order to gain insight into the understanding of multimode flutter and its generation mechanism. Through the use of an example long-span suspension bridge with a streamlined deck section, it is concluded that the dominant modes for most coupled flutter are the fundamental symmetric vertical and torsional modes. The coupled self-excited forces acting on the center span are the main source of negative damping that leads to flutter. Therefore, for the purpose of improving the flutter stability, it is important to reduce these destabilizing coupling effects. It is also emphasized that even in the case of relatively bluff deck sections, where the damping driven flutter dominated by a single mode would occur, the coupling effects may result in the occurrence of flutter prior to the onset velocity predicted by the conventional mode-by-mode approach.

The buffeting response of vertical and torsional motions indicates strong aerodynamic coupling at higher wind velocities. This coupling affects both the aerodynamic damping and the mode shapes. The conventional mode-by-mode method ignores the aerodynamic coupling among modes, which can lead to an underestimation of results. The cross spectra between different generalized buffeting forces seem to have little influence on the buffeting response even when the aerodynamic coupling is strong. Therefore, the cross spectra can be ignored for computational simplicity.

ACKNOWLEDGMENTS

The support for this work was provided in part by the Kyoto University, NSF Grants CMS 9402196 and CMS 95-03779. Their support is gratefully acknowledged. The writers are thankful to Fred Haan Jr., a doctoral candidate in the NatHaz Modeling Laboratory, for his comments on the manuscript.

APPENDIX. REFERENCES

Agar, T. T. A. (1989). ''Aerodynamic flutter analysis of suspension bridges by a modal technique.'' *Engrg. Struct.*, 11, 75–82.

Bleich, F. (1948). ''Dynamic instability of truss-stiffened suspension bridges under wind action.'' *Proc. ASCE*, 74(7), 1269–1314.

Davenport, A. G. (1962). ''Buffeting of a suspension bridge by storm winds.'' *J. Struct. Engrg. Div.*, ASCE, 88(6), 233–264.

Diana, G. (1993). ''Analytical and wind-tunnel simulations for the aeroelastic design of the Messina Straits Bridge.'' *Proc., Int. Sem. on Utilization of Large Boundary Layer Wind Tunnel*, Japan, 183–202.

Diana, G., Bruni, S., Collina, A., and Zasso, A. (1998). ''Aerodynamic challenges in super long span bridges design.'' *Bridge aerodynamics*, Larsen and Esdahl, eds., 131–144.

Jain, A., Jones, N. P., and Scanlan, R. H. (1996). ''Coupled flutter and buffeting analysis of long-span bridges.'' *J. Struct. Engrg.*, ASCE, 122(7), 716–725.

Karman, T. von, and Dann, L. G. (1949). ''Aerodynamic stability of suspension bridge.'' *Bulletin, No. 116*, Part 3, Engineering Experimental Stations, University of Washington, Seattle, Wash.

Karpel, M. (1982). ''Design for active flutter suppression and gust alleviation using state-space aeroelastic modeling.'' *J. Aircraft*, 19(3), 221–227.

Katsuchi, H., Jones, N. P., and Scanlan, R. H. (1999). ''Multimode coupled flutter and buffeting analysis of the Akashi-Kaikyo Bridge.'' *J. Struct. Engrg.*, ASCE, 125(1), 60–70.

Lin, Y. K., and Yang, J. N. (1983). ''Multi-mode bridge response to wind excitations.'' *J. Engrg. Mech.*, ASCE, 109(2), 586–603.

Matsumoto, M., Chen, X., and Shiraishi, N. (1994). ''Buffeting analysis of long span bridge with aerodynamic coupling.'' *Proc., 13th Nat. Symp. on Wind Engrg.*, Japan Association for Wind Engineering, 227–232 (in Japanese).
Matsumoto, M., and Chen, X. (1996). ''Time domain analytical method of buffeting response for long span bridges.'' *Proc., 14th Nat. Symp. on Wind. Engrg.*, Japan Association for Wind Engineering, 515–520 (in Japanese).
Matsumoto, M., Niihara, Y., Kobayashi, Y., Shirato, H., and Hamasaki, H. (1995). ''Flutter mechanism and its stabilization of bluff bodies.'' *Proc., 9th ICWE*, New Delhi, India, 827–838.
Miyata, T., and Yamada, H. (1988). ''Coupled flutter estimate of a suspension bridge.'' *Proc., Int. Colloquium on Bluff Body Aerodyn. and its Appl.*, Kyoto, 485–492.
Miyata, T., Tada, K., Sato, H., Katsuchi, H., and Hikami, Y. (1994). ''New findings of coupled flutter in full model wind tunnel tests on the Akashi Kaiko Bridge.'' *Proc., Symp. on Cable-Stayed and Suspension Bridges*, Deauville, France, 163–170.
Pfeil, M. S., and Batista, R. C. (1995). ''Aerodynamic stability analysis of cable-stayed bridges.'' *J. Struct. Engrg.*, ASCE, 121(12), 1784–1788.
Scanlan, R. H. (1978a). ''The action of flexible bridges under wind. I: Flutter theory.'' *J. Sound and Vib.*, 60(2), 187–199.
Scanlan, R. H. (1978b). ''The action of flexible bridges under wind. II: Buffeting theory.'' *J. Sound and Vib.*, 60(2), 201–211.
Scanlan, R. H. (1993). ''Problematic in formulation of wind-force models for bridge decks.'' *J. Struct. Engrg.*, ASCE, 110, 1433–1446.
Spanos, P. D., and Zeldin, B. A. (1997). ''Random vibration of system with frequency-dependent parameters or fractional derivatives.'' *J. Engrg. Mech.*, ASCE, 123(3), 290–292.
Wilde, K., and Fujino, Y. (1998). ''Aerodynamic control of bridge deck flutter by active surfaces.'' *J. Engrg. Mech.*, ASCE, 124(7), 718–727.
Xie, J., and Xiang, H. (1985). ''State-space method for 3-D flutter analysis of bridge structures.'' *Proc., Asia Pacific Symp. on Wind Engrg.*, India, 269–276.